Effect of Heat Treatment Combined with an Alternating Magnetic Field on Microstructure and Mechanical Properties of a Ni-Based Superalloy

CHUANJUN LI, MARTIN SEYRING, XI LI, YUNBO ZHONG, ZHONGMING REN, and MARKUS RETTENMAYR

The effect of a two-step heat treatment including solution and aging heat treatments in an alternating magnetic field (AMF) on microstructure and mechanical properties of the Ni-based superalloy DZ483 was investigated. In the solution heat treatment, the AMF significantly reduced the chemical segregation. In the aging heat treatment, the application of the AMF was found to not only modify the partition ratios of some elements like Al and Ti between the γ' precipitate and the γ matrix, but also to distinctly accelerate coarsening of γ' precipitates and to result in a larger mean particle size. Additionally, the morphology of γ' precipitates gradually evolved from a quasi cube without an AMF to a regular cubic shape in the AMF. Mechanical performance tests showed that hardness and tensile strength of the samples heat treated in the AMF were increased in comparison with those without an AMF. It is shown that the enhanced diffusivity in the AMF is mainly responsible for the change in microsegregation, particle size, and morphology evolution. Furthermore, the AMF promotes the solid solution strengthening and the order strengthening, both of which contribute to the improvement of mechanical properties.

https://doi.org/10.1007/s11661-019-05141-z

I. INTRODUCTION

Ni-BASED superalloys are widely applied in aero and industrial gas turbine engines owing to their high strength, excellent tensile, and fatigue strengths as well as their resistance to corrosive conditions at high temperatures. The excellent properties evidently depend on alloy composition and processing conditions during solidification and subsequent heat treatment. In general, as-cast superalloy components undergo a two-step heat treatment, *i.e.,* solution and aging heat treatments. The former is used to dissolve non-equilibrium microstructural constituents and to reduce the chemical segregation[1,2] and the latter is adopted to adjust morphology, size, and distribution of γ' precipitates in order to obtain an optimum mechanical performance.[3,4]

It is well known that directionally solidified superalloys have a heterogeneous dendritic structure with a certain fraction of γ/γ' eutectic. During solidification, some alloying elements such as Cr, Co, Mo, W, and Re segregate into the dendrite cores, whereas others like Al, Ti, and Ta segregate into the interdendritic region. Structural heterogeneities and chemical segregation severely degrade the mechanical properties of superalloys.[5,6] Therefore, it is necessary to dissolve the γ/γ' eutectic and to reduce chemical segregation as much as possible by a solution heat treatment. As a result, homogenization increases creep strength and ductility.[5] Additionally, coarse and incoherent γ' precipitates in the interdendritic region have to be dissolved in the γ matrix with the help of a solution heat treatment in order to afterwards re-precipitate fine, regular, and coherent γ particles. Traditional heat treatment routines can achieve the qualitative aspects of the above goals, but some conflicts in the optimization of properties arise. One example is that higher solution temperatures improve the creep properties at the expense of reduced tensile and fatigue strengths.[7] Another example is that

CHUANJUN LI is with the State Key Laboratory of Advanced Special Steel & Shanghai Key Laboratory of Advanced Ferrometallurgy & School of Materials Science and Engineering, Shanghai University, Shanghai 200072, P.R. China and also with the Otto Schott Institute of Materials Research, Friedrich-Schiller-Universität-Jena, 07743 Jena, Germany. Contact e-mail: cjli21@shu.edu.cn MARTIN SEYRING and MARKUS RETTENMAYR are with the Otto Schott Institute of Materials Research, Friedrich-Schiller-Universitt-Jena. XI LI, YUNBO ZHONG, and ZHONGMING REN are with the the State Key Laboratory of Advanced Special Steel & Shanghai Key Laboratory of Advanced Ferrometallurgy & School of Materials Science and Engineering, Shanghai University. Contact e-mail: zmren@staff.shu.edu.cn

Manuscript submitted September 4, 2018.
Article published online February 12, 2019

the total content of heavy alloying elements (Ta, W, and Re) has continuously increased in recently developed single-crystal superalloys.[6] Although this increases strength and creep resistance, it also results in lower diffusion rates during solution heat treatment, which in turn requires longer heat treatment times and/or higher temperatures. Taking the third-generation single-crystal CMSX-10 as an example, the total time and the highest temperature for solution heat treatment are about 45 h and 1638 K (1365 °C), respectively.[2] Solution heat treatment undoubtedly is time consuming and costly. Some attempts to optimize heat treatment procedures for a given superalloy have been undertaken to reduce the cost by adjusting temperatures and times, but the effort showed little success.[8]

The mechanical performance of directionally solidified superalloys also strongly depends on the subsequent aging heat treatment. It has been convincingly demonstrated that the shape and size of γ' precipitates significantly influence the creep properties.[9] An optimized aging heat treatment certainly has the potential to amend the creep properties.[4] Therefore, up to date, much effort has been devoted to developing the optimum heat treatment for different superalloys.[10–12]

Considering the level of sophistication of current heat treatments, it is by no means trivial to develop new heat treatment procedures that lead to an improvement of some properties and at the same time are not accompanied by the degradation of other properties.

Over the past decades, it was found that applying an alternating magnetic field (AMF) during materials processing can be an effective method to modify microstructures and properties of metallic materials. Numerous studies showed that an AMF can refine grains,[13] reduce the macro and/or microsegregation,[14,15] accelerate stress release,[16] and enhance diffusivity.[17,18] At present, AMFs are already widely applied in industrial production routines, *e.g.*, during continuous casting. In view of obvious advantages of AMFs such as contactless interaction and the variety of electromagnetic effects, some researchers applied AMFs to the heat treatment of light alloys and achieved a significant improvement of mechanical properties.[18–20] This demonstrates the high potential of AMFs for optimizing the heat treatment of alloys. Nevertheless, there are only few studies regarding the application of an AMF to the heat treatment of superalloys. Recently, we experimentally found that an AMF reduced the chemical segregation and enhanced the coarsening kinetics of γ' precipitates in the superalloy.[21]

Based on the earlier preliminary findings, the objective of this work is to systematically investigate the effect of the heat treatment in combination with an AMF on microstructure and mechanical properties of the directionally solidified superalloy DZ483. It is found that the AMF significantly modifies the morphology of γ' precipitates, reduces microsegregation, and improves the mechanical properties. Insight is given into the nature of the effects of an AMF on the morphological evolution of γ' precipitates and the mechanical properties of the superalloy.

II. EXPERIMENTAL PROCEDURE

A. *Materials*

A directionally solidified sample of the superalloy DZ483 was used in this work. Its chemical composition was Cr 11.88, Co 9.06, W 3.72, Mo 2.06, Al 3.48, Ti 3.92, Ta 4.94, C 0.074, and Ni in balance (in wt pct). The master alloy was melted in a vacuum induction melting furnace and then cast into an investment casting cluster mold consisting of six cylindrical bars of 16 mm in inner diameter and 230 mm in length. The bars were directionally solidified at a withdrawal rate of 6 mm/min, which led to columnar grains.

Some of the bars were cut into samples with dimensions of 8 mm in diameter and 5 mm in length, which were used for heat treatment with and without an AMF. Other bars were machined into standard samples for high-temperature tensile testing after heat treatment.

B. *Experimental Apparatus*

The AMF was produced by water-cooled copper coils through which a 50-Hz alternating current was passed. The AMF intensity could be adjusted in the range of 0 to 0.1 T by changing the electric current. The sample was placed in the region of maximum AMF intensity and simultaneously homogeneous temperature. The experimental apparatus for heat treatment in the AMF is schematically shown in Figure 1. Temperatures of both furnace and sample were monitored by *B* type thermocouples (Pt-30 pct Rh/Pt-6 pct Rh) with an accuracy of ± 1 K (± 1 °C). The samples resided in an Ar-filled quartz tube.

C. *Heat Treatment Schedule*

The heat treatment schedule for the DZ483 superalloy is given as follows: (1) solution treatment, 1477 K (1204 °C)/1 h → 1538 K (1265 °C)/1 h/air cooling (AC), (2) aging treatment, 1353 K (1080 °C)/(1 to 4) h/furnace cooling (FC), as displayed in Figure 2. A set of samples was heat treated in the AMF. Another set of samples underwent the same heat treatment, but in the absence of the AMF for comparison. One identical procedure except the AMF was used for solution heat treatment for all samples, whereas different aging times were used to observe the effect of the AMF on the morphological evolution of γ' precipitates.

D. *Characterization Methods*

The distribution of alloying elements in the samples after grinding and polishing was examined using energy dispersive X-ray spectroscopy (EDS) in a scanning electron microscope (SEM). In order to display the effect of the AMF on the microsegregation level of the alloying elements, the random sampling method proposed by Flemings *et al.*[22] and Gungor[23] (F–G method) was adopted. This method has been frequently utilized to characterize microsegregation in superalloys.[24] In this work, composition measurements were performed on 300 points on a rectangular grid. The grid

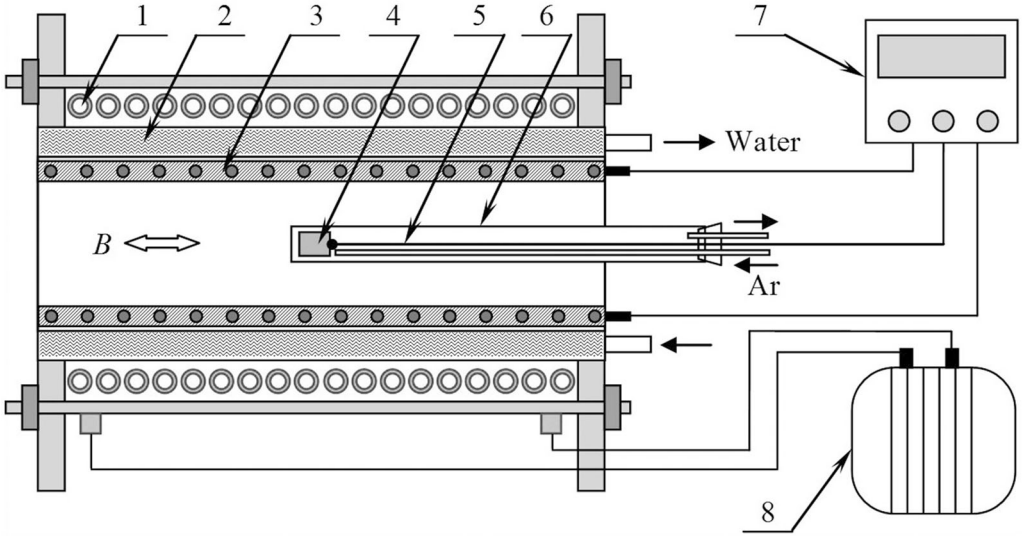

Fig. 1—Schematic illustration of the experimental set-up for heat treatment of the superalloy in the AMF, (1) copper coils, (2) water cooling jacket, (3) resistance furnace, (4) sample, (5) sample thermocouple, (6) quartz tube, (7) temperature controller, (8) voltage transformer.

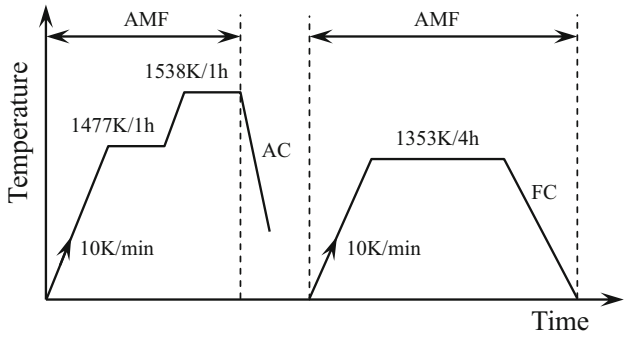

Fig. 2—Heat treatment schedule for superalloy DZ483 in the AMF.

spacing was 100 μm. The data for each element were sorted in ascending or descending order, depending on the segregation direction. The sets of ordered data were then converted to a characteristic non-dimensional microstructural length scale. Thus, a curve correlating composition with dimensionless length was obtained.

After electrolytic etching using a solution of 5 pct HNO_3 + 10 pct CH_3COOH + 85 pct H_2O, the dendrite structures were observed using an optical microscope. The morphology of the γ' precipitates was observed using the SEM. The edge lengths of all precipitates in more than four micrographs were measured using the software *Image-Pro Plus* and their arithmetic mean value was taken as the average particle size.

The lattice constants of the constrained γ and γ' phases and the partitioning behavior of the alloying elements between the two phases were examined using a transmission electron microscope (TEM) with an operating voltage of 300 kV. The thin foils for TEM observation were prepared by twin-jet electro polishing at 273 K and a voltage of 20 V using a solution of 69 pct C_2H_5OH + 5 pct $HClO_4$ + 11 pct $C_4H_9OC_2H_4OH$ + 15 pct H_2O. The constrained lattice misfits were determined by nano beam electron diffraction (NBED) using a beam diameter of 10 nm.[25] NBED patterns were recorded at four different positions in the γ matrix and in the γ' precipitates, respectively. The lattice constants for subsequent misfit calculation were measured and averaged over the relevant (200) and (400) reflections and anti-reflection positions in each NBED pattern.[26] The concentrations of the alloying elements in the γ matrix and the γ' precipitates were examined using EDS in the TEM. An elemental mapping and several point analyses were conducted using a probe size of 10 nm. The effect of the AMF on the partitioning behaviors of the elements was assessed using the partition ratio k, which is defined as $k = c_{\gamma'}/c_{\gamma}$, where $c_{\gamma'}$ and c_{γ} are the concentrations of the respective element in the γ' phase and the γ matrix, respectively. When $k > 1$, the element enriches in the γ' phase. When $k < 1$, the element enriches in the γ matrix. Measurements in 5 γ' precipitates and at 5 different positions of the γ matrix were performed. From these measurements, the average partition ratio for each element was calculated.

E. *Mechanical Performance Testing*

The Vickers hardness was determined by averaging the hardness values of six randomly selected positions.

Three tensile tests in each condition using standard samples were performed at 1223 K (950 °C) at a strain rate of 2.3×10^{-4}/s. The relevant mechanical properties such as tensile strength, elongation, and reduction in area were obtained. Fracture morphology and microstructure after the tensile tests were observed using a SEM.

III. RESULTS

A. *Microstructure*

Typical microstructures of directionally solidified DZ483 samples are shown in Figure 3. The highly heterogeneous structures consist of dendrites and γ/γ' eutectics in between (Figure 3(a)). The SEM micrographs reveal that large butterfly-like γ' precipitates consisting of eight small quasi cubes exist in the dendrite core (Figure 3(b)). The morphology of the γ' precipitates in the interdendritic region, which is markedly different from those in the dendritic core, shows numerous irregularly shaped cluster-like structures, each of which includes several (up to tens of) γ' precipitates (Figure 3(c)). For dissolving the γ/γ' eutectics and the γ' precipitates for subsequent uniform re-precipitation, an appropriate solution heat treatment was employed.

Figure 4 shows the morphology of γ' precipitates after solution heat treatment with and without an AMF. Under all conditions, the γ' precipitates have very similar morphology, *i.e.*, large butterfly-like γ' precipitates consisting of small quasi cubes. The splitting of large precipitates is well understood according to the elastic interaction between γ' precipitates.[27,28] However, the average size of the γ' precipitates in the AMFs is significantly larger than that without the field. Moreover, the mean particle size increases with increasing the AMF intensity. It is concluded that the application of an AMF stimulates re-precipitation and growth of γ' particles after solution heat treatment.

Following the solution heat treatment, an aging heat treatment was applied to adjust morphology, size, and distribution of γ' precipitates. Figure 5 shows the morphologies of the γ' precipitates after the aging heat treatment for different times with and without an AMF. From the morphology point of view, in the absence of the AMF, the γ' precipitates show quasi-cubic shape after an aging treatment for 1 hour (Figure 5(a)). The γ' precipitates gradually evolve from quasi cube to cube with increasing aging time (Figures 5(b) and (c)). For the short aging time, the AMF results in a morphology transition from quasi cube in 0 T to cube in 0.1 T (Figures 5(a), (d), and (g)). In the case of the longer aging times, the γ' precipitates show a cubic shape in 0.1 T in comparison with quasi cubes without an AMF (Figures 5(b) and (h)).

The change in shape can also be quantified using the shape factor F, which is defined as $F = 4\pi A/P^2$, where A and P are cross-sectional area and perimeter of the γ' precipitate, respectively. The shape factor varies in the range of 0 to 1 for thin elongated to spherical particles. The shape factor of a cube is 0.785. Figure 6 shows the variation of the shape factor with aging time and AMF intensity. Obviously, the application of the AMF reduces the shape factor, which in the present case quantitatively reflects the morphology transition from quasi cube to cube. From the perspective of the particle size, the mean size of the γ' precipitates evidently increases with increasing the aging time, irrespective of the AMF. For the same aging time, the mean particle

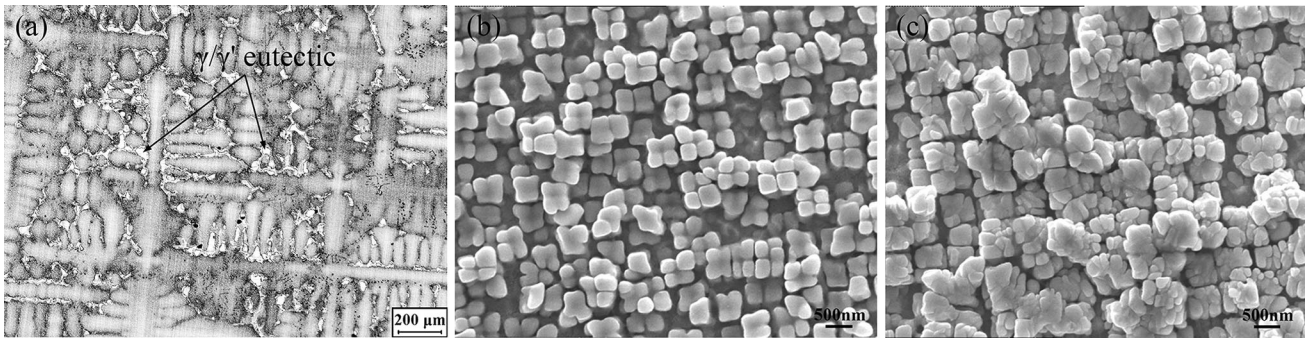

Fig. 3—Micrographs of the directionally solidified superalloy DZ483, (*a*) dendrite structures, (*b*) γ' precipitates in the dendrite core, (*c*) γ' precipitates in the interdendritic region.

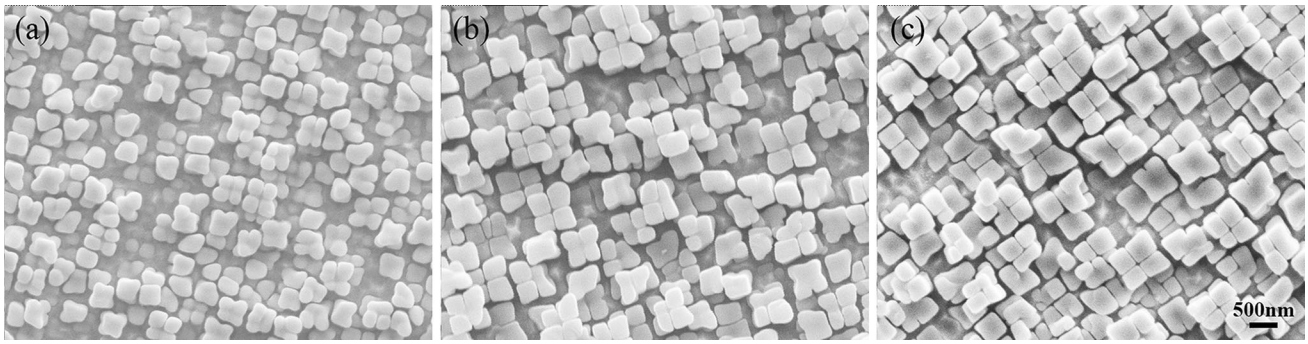

Fig. 4—Morphology of the γ' precipitates in the dendrite cores after solution heat treatment. (*a*) 0 T, (*b*) 0.065 T, (*c*) 0.1 T.

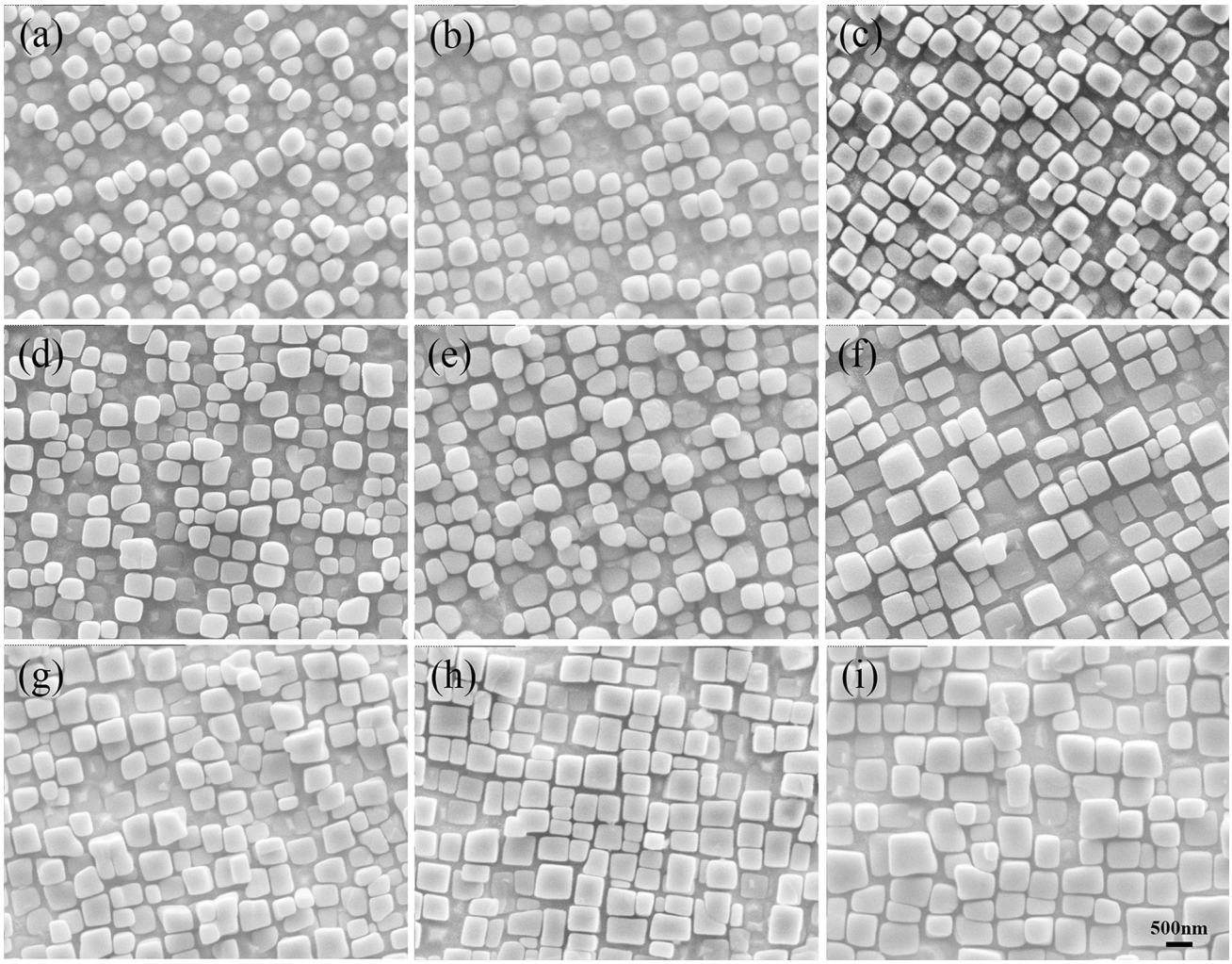

Fig. 5—Morphology of γ' precipitates after aging heat treatment for different aging times in various AMF intensities. (*a*) 1 h, 0 T, (*b*) 2 h, 0 T, (*c*) 4 h, 0 T, (*d*) 1 h, 0.065 T, (*e*) 2 h, 0.065 T, (*f*) 4 h, 0.065 T, (*g*) 1 h, 0.1 T, (*h*) 2 h, 0.1 T, (*i*) 4 h, 0.1 T.

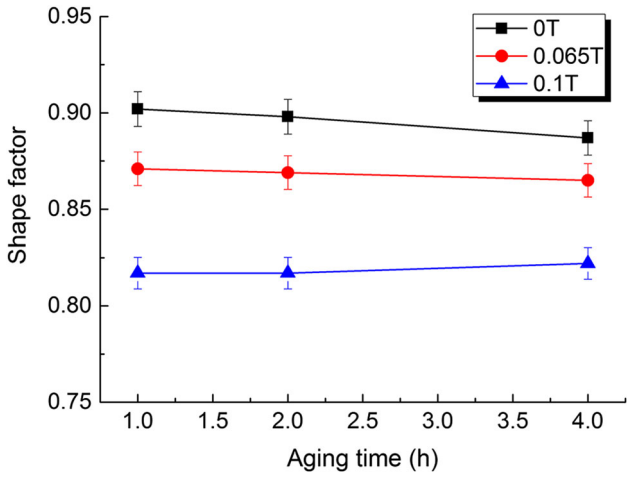

Fig. 6—Variation of the shape factor with AMF intensity and aging time.

sizes in the AMFs are larger in comparison with those without the AMF. A higher AMF intensity leads to a larger mean particle size. Additionally, the particle size distribution (PSD) is widened in the AMF, as displayed in Figure 7. This phenomenon is similar to the case of a broadened PSD at longer aging times.[29,30] It follows that the AMF not only results in a quasi cubic-to-cubic transition, and but also accelerates coarsening of γ' particles during the aging heat treatment.

B. *Composition*

In order to compare the severity of microsegregation after heat treatment with and without an AMF, the composition profiles characterizing microsegregation are plotted against the dimensionless length, as shown in Figure 8. These curves reflect the variation of concentrations of the alloying elements from the dendrite core to the interdendritic region. According to their

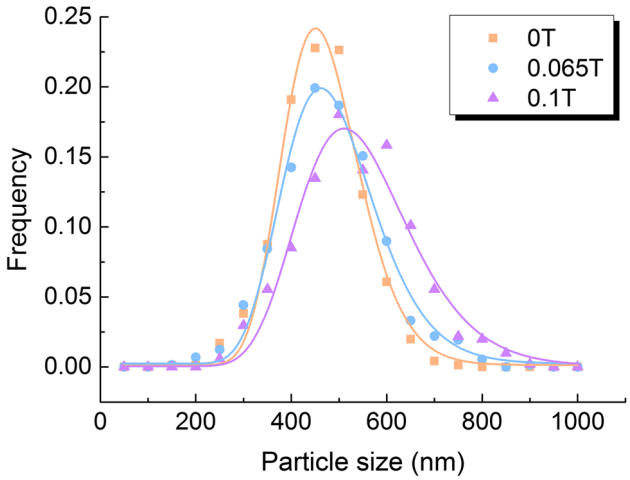

Fig. 7—Log-normal distributions of γ' particle sizes after aging treatment for 4h in different AMF intensities.

segregation directions, the concentration profiles can be divided into two groups. The first group consists of the alloying elements Al, Ti, Ta, and Ni featuring increasing concentration with the normalized length. These elements preferentially segregate to the melt during primary solidification. The second group consists of the elements Cr, Co, Mo, and W, showing inverse segregation. It should be noted that the segregation directions of the element Cr in some superalloys may vary with processing steps (from solidification to solution heat treatment) owing to the cross diffusion effect,[31] which is not the case in the current investigation. During solid solution treatment, the first group of elements diffuses from the interdendritic region to the dendrite core while the second group diffuses in an inverse direction. As homogenization proceeds, the concentrations of alloying elements in the dendrite core (low dimensionless length) and the interdendritic region (high dimensionless length) progressively approach the average composition, *i.e.,* the normalized concentration profiles gradually approach unity. In Figure 8, as shown, the normalized concentration profiles of all elements in the AMF of 0.1 T are closer to unity than those without an AMF. The feature is especially obvious near low and high dimensionless lengths. This indicates that the AMF accelerates homogenization and reduces the extent of microsegregation.

The amount of microsegregation of the alloying elements can be further quantified using the segregation coefficient, which is defined as the ratio of the concentration of the element in the dendrite core to that in the interdendritic region. Figure 9 displays the segregation coefficients of elements with and without the AMF of 0.1 T. The application of the AMF results in larger segregation coefficients of Al, Ti, Ta, and Ni and reduces the segregation coefficient of Cr, Co, Mo, and W. Anyway, the segregation coefficients of all elements in the AMF are closer to unity, which coincides with the change in the composition profiles. This demonstrates that the application of an AMF leads to a more homogeneous distribution of alloying elements. In addition, the amount of the residual eutectics which reflects the homogenization level after solution heat treatment was also examined. The statistical analysis showed that the volume fractions of the residual eutectics in the samples that were solution heat treated in 0, 0.065 and 0.1 T are 1.05, 0.98, and 0.93 pct, respectively, *i.e.*, the amount of the residual eutectics in an AMF is slightly less than that without an AMF. Therefore, it can be concluded that the AMF can effectively reduce the microsegregation level during solution heat treatment.

Additionally, the effect of the AMF on the partitioning behavior of the alloying elements between the γ' precipitate and the γ matrix was examined using the TEM. Figure 10 shows composition maps of DZ483 after the aging heat treatment without an AMF, which qualitatively displays the partitioning behavior of various elements. The elements Al, Ti, Ta, and Ni are preferentially found in the γ' precipitates, whereas the elements Cr, Co, Mo, and W are preferentially partitioned in the γ matrix. The partitioning behavior of the elements in DZ483 is the same as in other superalloys such as SRR99[32] and CMSX-4.[33] In the AMF, the partitioning of different alloying elements shows the same tendency as that without an AMF. However, the partition ratios of some elements with and without an AMF exhibit differences, as shown in Figure 11. The partition ratios of the elements Al and Ti in the AMF increase, whereas the other elements show no obvious change except for the slight change in the partition ratios of Ta and Mo. This means that the content of γ'-forming elements such as Al and Ti in the γ' precipitates increases in the AMF, which leads to increase in the lattice constant of the γ' phase.[34] The change in the partition ratios should modify the lattice misfit δ, defined as $\delta = 2(a_{\gamma'} - a_{\gamma})/(a_{\gamma'} + a_{\gamma})$, where $a_{\gamma'}$ and a_{γ} are the lattice constants of the γ' and γ phases, respectively. The TEM diffraction analysis shows that in the dendrite core δ is $(5.38 \pm 3.95) \times 10^{-3}$ without an AMF and $(4.44 \pm 3.52) \times 10^{-3}$ with 0.1 T. According to the small difference of mean values of the measured lattice misfits with and without an AMF in combination with their relative strong experimental deviation, a significant impact of the AMF on misfit cannot be identified.

C. *Mechanical Properties*

Figure 12 shows the variation of the Vickers hardness with AMF intensity after aging. The plots indicate a significant effect of the AMF on hardness. For the same aging time, the AMF increases the hardness of all the DZ483 samples. Moreover, a stronger AMF results in a higher hardness. For example, the increase in hardness in 0.065 and 0.1 T are up to 3.2 and 8.2 pct after aging treatment for 4 hours, respectively.

Table I shows the tensile properties of the DZ483 samples after aging heat treatment with and without AMF. The tensile strengths of the samples after aging treatment in 0.065 and 0.1 T increase by 2.3 and 4.5 pct,

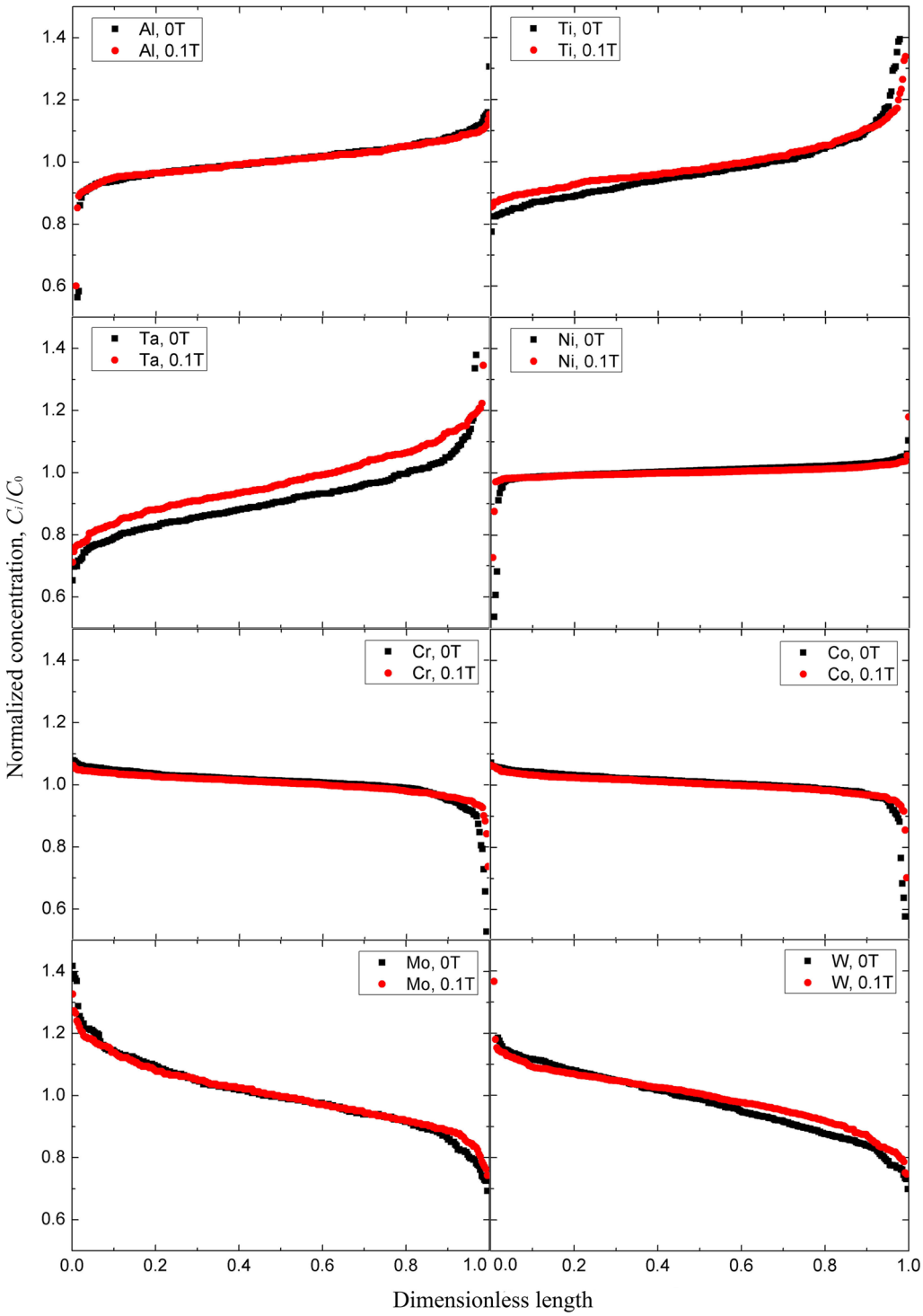

Fig. 8—Normalized composition profiles of alloying elements in DZ483 after solution heat treatment according to the F–G method. C_i and C_0 are the measured concentration and the average concentration of each alloying element, respectively.

respectively, in comparison with that in 0 T. As expected for the higher strengths, elongation and the reduction in area in the AMFs are reduced.

The fracture morphology of the DZ483 samples with and without AMF displays little change, as shown in Figure 13. The fracture surfaces of the samples with and without an AMF all exhibit a large number of dimples. Thus, the fracture mechanism is essentially ductile for the DZ483 samples, regardless of the AMF.

Figure 14 shows the morphology of γ' precipitates in deformed regions of the DZ483 samples after tensile testing at 1223 K (950 °C). Similar to the change of the initial microstructure after aging heat treatment, the average particle size in the samples heat treated in the

AMF is larger than that without the AMF. Additionally, there are three main features in the deformed regions of all samples. The first one is that most of the γ' particles are elongated along the direction of deformation owing to the uniaxial tensile stress. The second one is that rafts perpendicular to the stress direction begin to form, which originates from the negative lattice misfit.[35,36] Owing to the relatively short time for the tensile tests at the high temperature, the present rafts only exhibit chain-like structures, which are similar to the morphology of rafts at the initial stage of rafting during creep.[37] The last one is that the width of matrix channels parallel to the rafts significantly increases. Nevertheless, these three features show no obvious difference between samples with and without an AMF. It should be noted that the lattice misfit of DZ483 changed from a positive misfit at room temperature to a negative misfit at high temperatures due to the

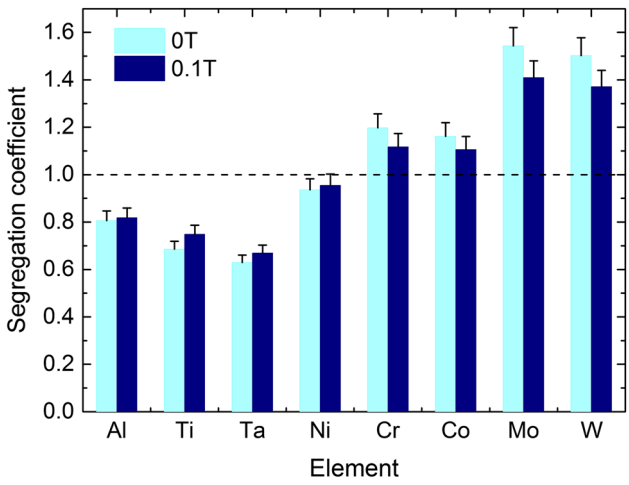

Fig. 9—Segregation coefficients of the elements in DZ483 after solution heat treatment with and without an AMF of 0.1 T.

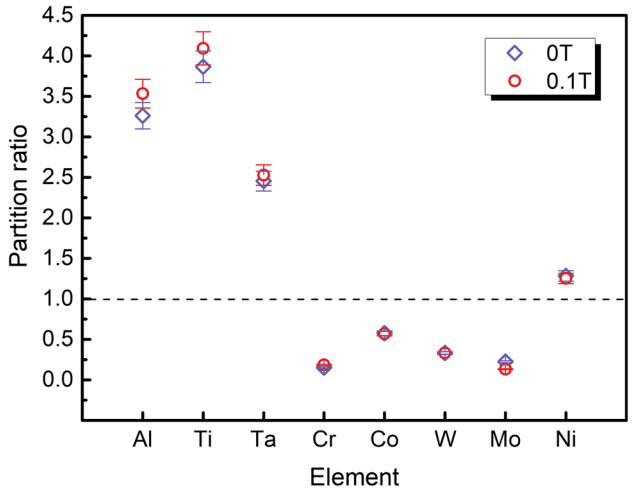

Fig. 11—Partition ratios of alloying elements in DZ483 after aging heat treatment for 4 h with and without an AMF of 0.1 T.

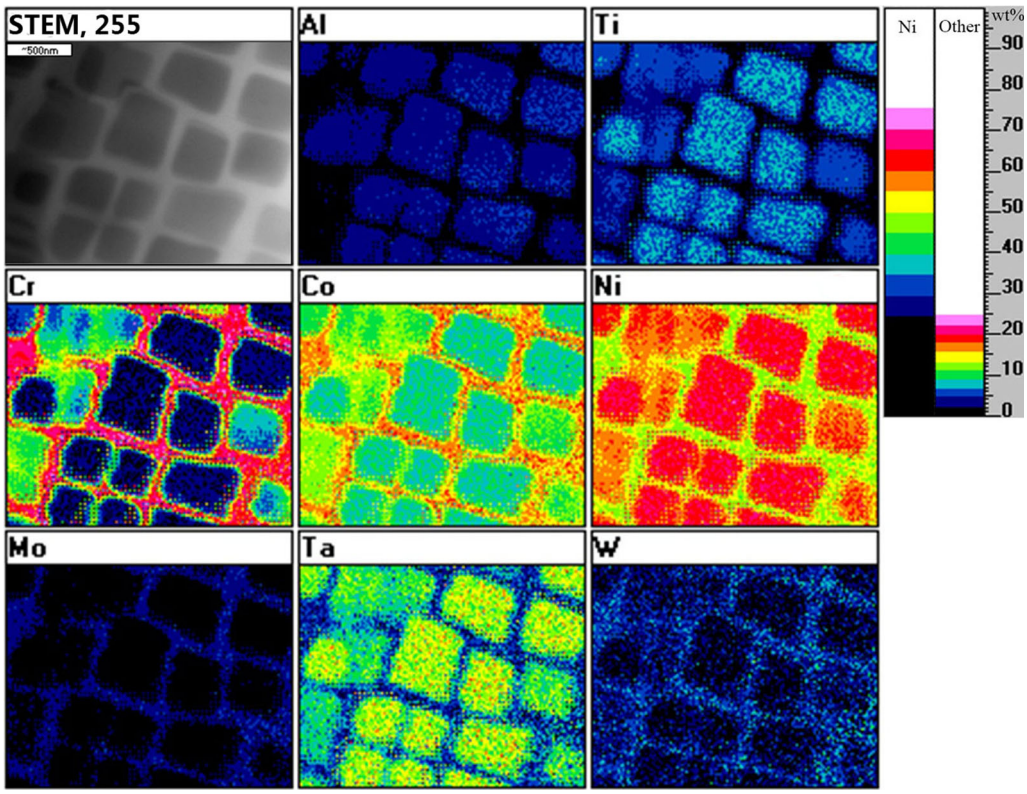

Fig. 10—Composition maps in the superalloy DZ483 after aging heat treatment for 4h without an AMF.

larger thermal expansion coefficient of the matrix with respect to the precipitate, which commonly occurs in superalloys.[33]

IV. DISCUSSION

From the foregoing results, it can be seen that the application of the AMF during heat treatment reduced the severity of microsegregation, accelerated coarsening of γ' precipitates, enhanced the morphological transition from quasi cube to cube, and finally improved the mechanical properties of the superalloy DZ483. In the following, the effects of the AMF on microstructure and mechanical properties are discussed.

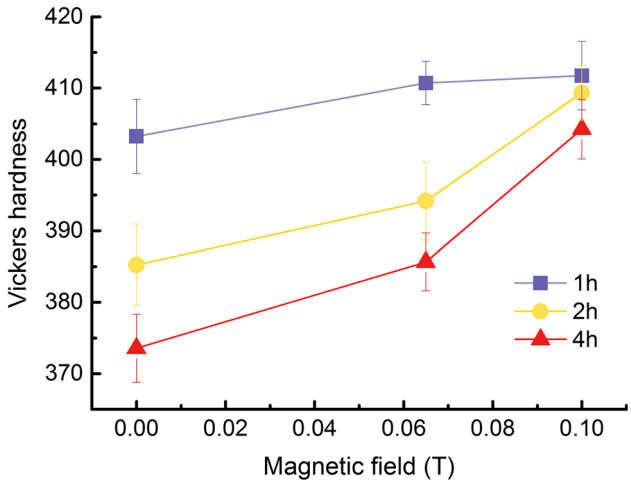

Fig. 12—Vickers hardness of the DZ483 samples after aging heat treatment with and without an AMF.

A. *Coarsening Kinetics of γ' Precipitates*

It is well known that growth and coarsening of γ' precipitates are controlled by diffusion. The coarsening kinetics can be described by the Lifshitz–Slyozov–Wagner (LSW) theory.[38,39] In this theory, the average particle size increases with time according to the relationship,

$$d^3 - d_0^3 = kt. \quad [1]$$

In Eq. [1], d and d_0 can be interpreted as the edge lengths of cubic γ' precipitates at the time t and $t = 0$, respectively; k is the rate constant and given by $k = 64\sigma V_m^2 D C_e/(9RT)$, where σ is the γ/γ' interfacial free energy, V_m is the molar volume of the γ' precipitate, C_e is solute concentration, R is the universal gas constant, and T is the temperature. The above equation shows how the coarsening rate of γ' precipitates is influenced by several entities. It is of high importance to determine the difference between the rate constants with and without an AMF.

It has been shown that an AMF can influence the interfacial properties. A significant impact has been shown for ferromagnetic materials, where an increase in the interfacial free energy between ferrite and cementite resulted in a morphological transition of the carbide.[40] According to the interface model proposed by Zhang *et al.*,[40] the change in the interfacial free energy σ^M induced by a magnetic field can be expressed as

$$\sigma^M = \frac{\delta_i}{2}(\Delta G_\gamma^M + \Delta G_{\gamma'}^M),$$

where ΔG_γ^M and $\Delta G_{\gamma'}^M$ are the magnetic Gibbs free energies per unit volume of the γ and γ' phases, respectively, reduced by the magnetic field, and δ_i is

Table I. Tensile Properties of the DZ483 Samples After Aging Treatment for 4 h With and Without AMFs

B(T)	Tensile Strength (MPa)	Elongation (Percent)	Reduction in Area (Percent)
0	663 ± 2.5	22.2 ± 2.3	34.0 ± 1.8
0.065	678 ± 2.7	18.7 ± 2.5	31.7 ± 2.2
0.1	693 ± 3.2	20.4 ± 1.4	31.6 ± 2.4

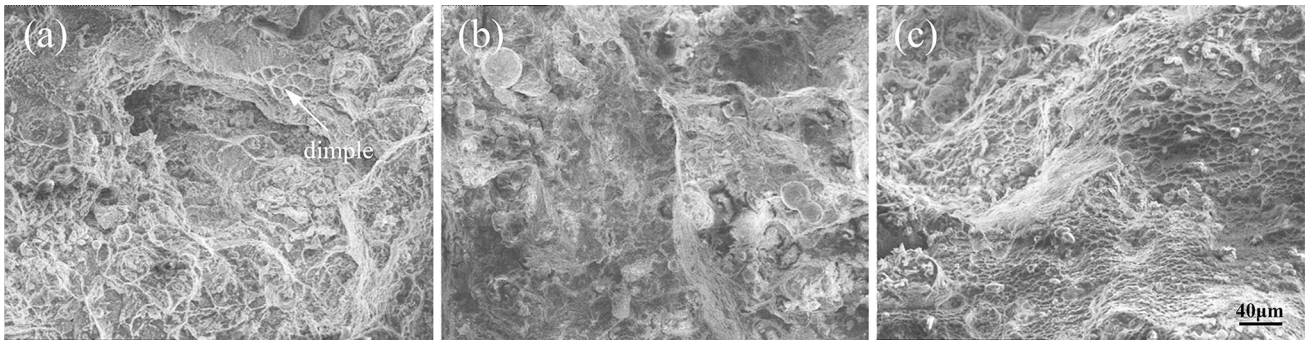

Fig. 13—Fracture morphology of the DZ483 samples after tensile testing at 950 °C. (*a*) 0 T, (*b*) 0.065 T, (*c*) 0.1 T.

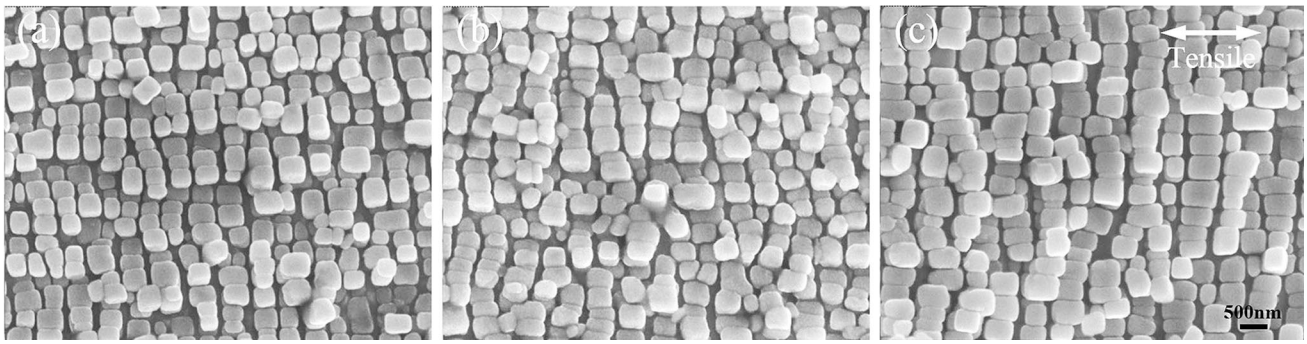

Fig. 14—Morphology of γ' particles after tensile testing in deformed regions of the DZ483 samples heat treated with and without AMFs. (*a*) 0 T, (*b*) 0.065 T, (*c*) 0.1 T.

the thickness of the γ/γ' interface. The magnetic Gibbs free energy can be expressed as $\Delta G^{M} = -\chi B^2/2\mu_0$, where χ, B and μ_0 are the volume magnetic susceptibility, the magnetic flux density, and the vacuum magnetic permeability.

Considering the magnetic susceptibilities of pure Ni[41] and Ni_3Al[42] together with the interface thickness of 3.59 nm,[43] σ^{M} can be calculated to be 7.5×10^{-9} J/m^2 in the AMF of 0.1 T. Compared with the γ/γ' interfacial free energy of 6.9×10^{-3} J/m^2,[44] σ^{M} is about six orders of magnitude smaller than the interfacial free energy. It follows that the change in the interfacial free energy in the AMF does not contribute significantly to the coarsening rate of the γ' precipitates.

Nevertheless, the AMF was found to increase the diffusion rates of some alloying elements such as Al[45] and Cr.[46] For example, the interdiffusion coefficients in the Ni–Al alloys at 1353 K (1080 °C) without and with 0.1 T are calculated to be 7.04×10^{-15} and 1.24×10^{-14} m^2/s, respectively. The details regarding the change in diffusivity in an AMF have been investigated in previous work and documented in the literatures.[45,46] The enhanced diffusivity in the AMF necessarily accelerates coarsening of γ' precipitates. It is worth pointing out that the interaction of different diffusing elements (superalloys generally include more than 10 alloying elements[47]) will change the diffusion rate of each element.

As for the molar volume of the γ' phase, since the γ and γ' phases are both paramagnetic at the aging temperature, there is no magnetostriction effect for the γ' phase at the aging temperature and thus the molar volume should not change in the AMF. The last parameter to be discussed is the equilibrium concentration C_e in the matrix. The measurements show that the concentrations of γ'-forming elements like Al, Ti, and Ta in the matrix in the AMF are lower than those without AMF. For example, C_e of Al is measured to be 3.42 and 2.69 at.pct in the samples heat treated without and with 0.1 T, respectively.

Considering the change in these factors, the coarsening kinetics of γ' precipitates with and without an AMF can be calculated using Eq. [1], resulting in curves in Figure 15. Obviously, under the assumption of independent diffusion, the coarsening rate in the AMF is faster than that without an AMF, which is in qualitative

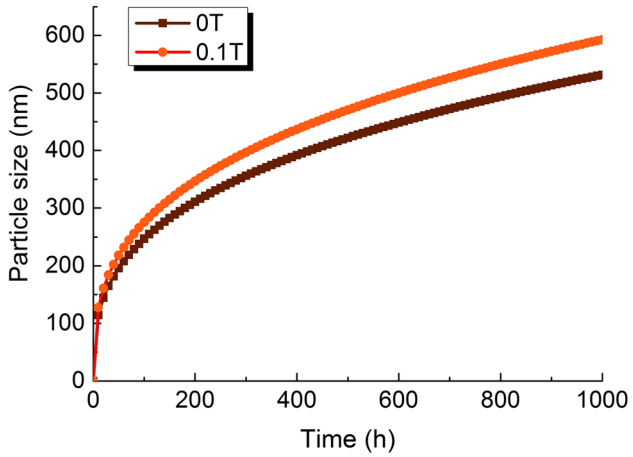

Fig. 15—Variation of the particle size with aging time with and without the AMF of 0.1 T as calculated by Eq. [1], the following parameters are used: $d_0 = 0$ nm, $\sigma = 6.9 \times 10^{-3}$ J/m^2,[44] $V_m = 6.79 \times 10^{-6}$ m^3/mol, C_e of Al were measured to be 3.42 and 2.69 at. pct without and with 0.1 T, D is taken as 1.24×10^{-14} and 7.04×10^{-15} m^2/s at 1353 K (1080 °C) with and without 0.1 T, respectively.[45]

agreement with experimental observation. Here we do not compare the experimental results to the calculation. The reasons are that the exact values of some parameters like the γ/γ' interfacial free energy and the interdiffusion coefficients of the alloying elements in DZ483 are not known with sufficient detail. The LSW theory only holds for very low volume fractions of spherical precipitates. In almost all studies regarding the coarsening kinetics of γ' precipitates in commercial superalloys, the experimental data of the particle size *vs* the coarsening time were fitted, and further proper values for the coarsening kinetics equation were chosen.[48,49] Furthermore, the coarsening kinetics may strongly deviate from predictions of the LSW theory owing to special phenomena such as splitting during coarsening.[28] Further coarsening experiments in the AMF are in progress.

The elastic energy due to the lattice misfit also contributes to the coarsening rate of γ' particles. Ardell showed how the coarsening rate increased at a given aging temperature with increasing lattice misfit.[50] Nevertheless, as shown above, the difference in lattice

misfits with and without an AMF is not distinct. Thus, the change in elastic energy due to the AMF does not significantly alter the coarsening rate of γ' precipitates.

B. *Morphological Evolution of γ' Precipitates*

The morphological evolution of γ' precipitates in superalloys has been widely studied, and various morphologies like sphere, cube, plate, raft, and dendrites have been observed.[27,51–53] It is well understood that the γ' morphology is closely related to particle size and lattice misfit as well as elastic interaction between precipitates.[27,52] In this work, the AMF exerted a pronounced effect on the morphology of γ' precipitates during solution and aging heat treatment. In the following, the morphology evolution in the AMF during the two annealing stages is discussed separately.

During solution heat treatment, alloying elements such as Al, Ti, and Ta, which segregate into the interdendritic region during primary solidification, gradually diffuse into the dendrite cores, whereas other alloying elements such as Cr, Co, Mo, and W, which segregate into the dendrite core, diffuse from the dendrite core to the interdendritic region. Additionally, the γ' phase completely dissolves in the γ matrix at the solution temperature, which leads to a supersaturated solid solution upon cooling. Since the enhanced diffusivity under the action of the AMF results in higher concentrations of γ'-forming elements in the dendrite core compared with those without an AMF before complete homogenization, the supersaturation of γ'-forming elements in the dendrite core in the AMF is higher than that without an AMF. Correspondingly, the driving force for precipitation of γ', which depends on the supersaturation,[54] becomes larger in the AMF. Under the same cooling conditions, the γ' precipitates in the AMF thus grow faster than those without an AMF. Therefore, the average size of γ' precipitates in the samples that were solution treated in the AMF was larger, although the samples had been removed from the AMF during cooling.

As the γ' precipitates grow, they split after reaching a critical size due to the accumulated elastic strain energy caused by the lattice misfit. It was theoretically shown that the following morphology evolution occurs as the growth proceeds: sphere $\rightarrow$ cube if $d \geq 7.7a_0$, cube $\rightarrow$ doublet if $d \geq 27a_0$, doublet $\rightarrow$ octet if $d \geq 82a_0$, and octet $\rightarrow$ platelet if $d \geq 377a_0$, where a_0 is the ratio of the interfacial free energy to the elastic strain energy.[27] In the case of Ni_3Al, the critical sizes for sphere $\rightarrow$ cube and cube $\rightarrow$ octet are predicted to be 7.7 and 55 nm, respectively.[27] In the present work, concluding from the morphology of γ' precipitates after solution heat treatment (Figure 4), the critical size for sphere $\rightarrow$ cube transition is not straightforward to be determined precisely, but estimated to be in the range of 200 to 300 nm, which approximately coincides with previous experimental observations in a single-crystal superalloy in which the transition from spherical to cubic γ' occurred at a size of about 300 nm.[9] It is worth noting the transition sphere $\rightarrow$ cube is fast in the case of an interfacial reaction, which renders the above value range to be rather approximate. However, a theoretical estimation of a_0 values shows that the critical sizes with and without an AMF are almost identical, because there are no obvious changes in both the lattice misfit and the γ/γ' interfacial free energy.

Additionally, it can clearly be seen that γ' precipitates underwent splitting from cube to octet, which was also observed in other Ni-based superalloys.[55] In the absence of the AMF, the majority of γ' precipitates just began to split, whereas in the AMF most γ' precipitates had finished splitting owing to their larger sizes. It is shown that the critical size for splitting in DZ483 is about 380 to 420 nm, which is much larger than the above-mentioned theoretical prediction of 55 nm. It is not surprising that a significant deviation between theoretical calculation and experimental observation exists, since the theoretical model has several restricting assumptions, as pointed out by the authors.[27] For different superalloys, the critical sizes for splitting are different. For example, Miyazaki *et al.* found a critical size for splitting of Ni_3Al precipitates of ~800 nm.[56] At any rate, a larger size is beneficial for splitting in a given superalloy, and the AMF speeds up the progress of splitting.

For the subsequent aging heat treatment, the initial microstructure is "inherited" from the solution heat treatment. Some γ' precipitates which did not split or incompletely split continued to split into individual particles at the aging temperature and then all individual particles continue to coarsen. The average particle size in the AMF becomes larger with respect to the condition without an AMF due to enhanced diffusivity. Owing to the elastic interaction between precipitates, splitting is suppressed, and the rearrangement of γ' precipitates along the softest [001] direction is preferred to reduce the elastic energy.[57] Since the elastic energy, which increases with increasing the particle size, favors faceted growth of γ' precipitates along the softest plane of 001, the application of the AMF enhances the transition tendency from rounded cube to perfect cube.

C. *Mechanical Properties*

The current experimental results show how the application of the AMF during heat treatment of the DZ483 samples improves mechanical properties such as hardness and the tensile strength. Since one of the pronounced differences between low- and high-temperature deformation is that dislocation formation and expansion starts in the γ' precipitate at low temperatures and in the γ matrix at high temperatures,[58] we discuss the change in hardness and high-temperature tensile strength in the AMF, respectively.

As we know, directionally solidified superalloys that consist of γ and γ' are mainly strengthened by two strengthening mechanisms, *i.e.,* solid solution strengthening of the γ matrix and precipitation strengthening of γ' phase.

For solid solution strengthening, the strengthening effect depends on a variety of factors such as difference in atomic sizes, local difference in shear modulus, change in stacking fault energy, long-range or

short-range ordering.[59] The alloying elements will strengthen the γ matrix to different extents. For the DZ483 superalloy under investigation, Mo and W undoubtedly played a crucial role in solid solution strengthening,[60] since the concentration of γ' forming elements in the γ matrix was strongly reduced due to the precipitation of the γ' phase. The increase in the partition ratios of Al and Ti in the AMF implies that the relative contents of W and Mo in the matrix increase. Thus, the change in the partition ratios of the alloying elements strengthens the γ matrix.

For precipitation strengthening, the γ' precipitates can impede the motion of dislocations through various interaction mechanisms including the stacking fault strengthening, modulus hardening, coherency strengthening, and order strengthening.[61] Although those mechanisms are likely to be operative simultaneously in Ni-based superalloys, the contribution from order strengthening outweighs other contributions from other strengthening effects.[62]

Order strengthening occurs if a matrix dislocation tries to shear an ordered precipitate. Based on the shearing interaction between a dislocation and precipitates, Reppich developed a model of precipitate hardening at low temperatures for large volume fractions of precipitates.[63] In this model, when the particle size is large enough, the critical resolved shear stress (CRSS) $\Delta\tau_0$ which causes the leading dislocation to penetrate into the γ' precipitate is expressed as

$$\Delta\tau_0 = \frac{\gamma_0}{b} - \frac{\sqrt{6}T}{bd}, \qquad [2]$$

where γ_0 is the anti-phase domain boundary energy of γ' precipitates; b is the Burgers vector of the edge dislocation in the matrix; and T is the line tension of the dislocation. The line tension of dislocation can be approximated by

$$T = Gb^2/2. \qquad [3]$$

In the above equation, G is the shear modulus. Combining Eqs. [2] and [3], the penetration stress is rewritten as

$$\Delta\tau_0 = \frac{\gamma_0}{b} - \sqrt{\frac{3}{2}}\frac{Gb}{d}. \qquad [4]$$

When the particle size is larger than a critical value d_c, the Orowan by-passing process is favored since the Orowan stress is less than the penetration stress. For anisotropic materials, the Orowan stress for screw dislocations which are more difficult to bend than edge dislocations is given as[63]

$$\Delta\tau_a^{\text{screw}} = \left(\frac{K_E b}{2\pi L}\right) \cdot \ln\left(\frac{2\bar{d}}{b}\right) \cdot \left[\frac{\ln\left(\frac{2\bar{d}}{b}\right)}{\ln\left(\frac{l_{OR}}{b}\right)}\right]^{1/2}, \qquad [5]$$

where K_E is the line energy factor of the edge dislocation; L is the mean planar interparticle spacing of particles with diameter d and the volume fraction f; and $L = d\left(0.724f^{-1/2} - 0.816\right)$, $\bar{d}$ is the harmonic mean of d and L, *i.e.*, $\bar{d} = (1/d + 1/L)^{-1}$.[64] l_{OR} is the particle spacing along a dislocation located in the Orowan configuration and it can be estimated as $l_{OR} = L \cdot \left[\ln\left(\frac{l_{OR}}{b}\right)/\ln\left(\frac{2\bar{d}}{b}\right)\right]^{1/2}$.

Combining Eqs. [4] and [5], the critical size d_c can be estimated to be 567 nm for the DZ483 superalloy using the following values: f = 0.6, b = 0.254 nm, K_E = 105 GPa,[63] γ_0 = 0.111 J/m^2,[65] and G = 57 MPa.[66] The critical size is larger than all average particle sizes in different aging conditions and the CRSS increases with increasing the particle size. Since the Vickers hardness test can produce a strain of up to 7 pct,[67] the estimation of the change in CRSS with the particle size coincides with experimental observation of hardness.

As for the tensile tests, it has been well established that the deformation mechanism is shearing of γ' particles at low temperatures and particle by-pass at high temperatures, respectively. The transition from shearing to by-pass occurs at intermediate temperatures.[68] Additionally, the strain rate also influences the deformation mechanism.[58] For tensile tests at high temperatures and relatively low strain rates (*e.g.*, 10^{-4}/s), the dislocations firstly expand from the matrix, which leads to the formation of dislocation network at the γ/γ' interface, After a period of hardening, softening occurs by shearing of γ' particles and by diffusional processes.[58] Shearing of large particles will evidently be more difficult as compared to the small particles. In this case, a larger mean particle size improves the tensile strength at the high temperature in a certain range of particle sizes. This is in accordance with experimental observations by Sentupta *et al.*,[69] who compared the tensile properties of differently heat-treated CMSX-4 samples with the three mean particle sizes (*i.e.*, 300, 500, and 900 nm) at room and elevated temperatures. It was shown that the tensile strength increased with increasing the mean particle size at temperatures below 800°C. At the temperatures above 800°C, the tensile strength of the samples with mean particle size of 500 nm was the highest. Additionally, the creep tests at 1000°C showed that the creep life showed a peak as the mean initial particle size increased and the optimum creep resistance appeared in the sample with the mean particle size of about 450 to 500 nm when the superalloy has an intermediate mismatch (0.1 to 0.5 pct).[9] It follows that the tensile and creep strengths at high temperatures show an optimum value with an increase in mean particle size. For DZ483, its misfit was measured to be about 0.4 to 0.5 pct. Therefore, it may be inferred that the tensile strength and the creep resistance of the superalloy DZ483 at a high temperature should show a peak with an increase in particle size. In combination with the current experimental results, the mean particle size in the AMF of 0.1 T is the largest and correspondingly the tensile strength is the highest. This means that the average particle size in 0.1 T is closest to the optimum size. Accordingly, an AMF results in a larger

mean particle size and further improves the tensile strength of the superalloy at the high temperature.

V. CONCLUSION

When an AMF is applied during heat treatment of the superalloy DZ483, the microstructure and the composition are considerably modified and the mechanical properties are also improved. The main conclusions can be drawn as follows.

1. The AMF accelerates growth and coarsening of γ' precipitates during heat treatments. Thus the average particle size in an AMF is larger than that without an AMF. Additionally, the AMF enhances the γ' morphology transition from quasi cubic to cubic. These phenomena mainly originate from the enhanced diffusivity in the AMF.
2. The application of an AMF during heat treatment leads to a less pronounced microsegregation than without an AMF. The AMF also changes the partition ratios of some elements such as Al and Ti, which does not significantly modify the lattice misfit between γ' precipitates and γ matrix.
3. Heat treatment in an AMF increases the Vickers hardness and the high-temperature tensile strength of DZ483. In addition to the solution strengthening of the γ matrix owing to change in partition ratios of elements, a larger mean particle size increases the CRSS and thus the Vickers hardness in the regime of the cutting mechanism at low temperatures. High-temperature tensile strength is also improved.

ACKNOWLEDGMENTS

One of the authors (C. Li) is very grateful for support from the Alexander von Humboldt Foundation. This work was also supported by Shanghai Pujiang Talents Program (18PJ1403700), the Natural Science Foundation of China (Grant Numbers 51401116, 51690162, and U1560202), and the United Innovation Program of Shanghai Commercial Aircraft Engine (Grant Nos. AR910, AR911).

REFERENCES

1. X. Huang, M.C. Chaturvedi, and N.L. Richards: *Metall. Mater. Trans. A*, 1996, vol. 27A, pp. 785–90.
2. G.E. Fuchs: *Mater. Sci. Eng. A*, 2001, vol. 300, pp. 52–60.
3. J.J. Jackson, M.J. Donachie, M. Gell, and R.J. Henricks: *Metall. Trans. A*, 1977, vol. 8A, pp. 1615–20.
4. P. Caron and T. Khan: *Mater. Sci. Eng.*, 1983, vol. 61, pp. 173–84.
5. G.E. Fuchs: *J. Mater. Eng. Perform.*, 2002, vol. 11, pp. 19–25.
6. H. Pang, N. D'Souza, H. Dong, H. Stone, and C. Rae: *Metall. Mater. Trans. A*, 2016, vol. 47A, pp. 889–906.
7. K.R. Bain, M.L. Gambone, J.M. Hyzak, and M.C. Thomas: *Superalloys*, 1988, vol. 1988, pp. 13–22.
8. B.C. Wilson, J.A. Hickman, and G.E. Fuchs: *JOM*, 2003, vol. 55, pp. 35–40.
9. M.V. Nathal: *Metall. Trans. A*, 1987, vol. 18A, pp. 1961–70.
10. J. Andersson, G.P. Sjöberg, L. Viskari, and M. Chaturvedi: *Mater. Sci. Technol.*, 2013, vol. 29, pp. 43–53.
11. D.U. Furrer, R. Shankar, and C. White: *JOM*, 2003, vol. 55, pp. 32–34.
12. H. Pang, L. Zhang, R. Hobbs, H. Stone, and C. Rae: *Metall. Mater. Trans. A*, 2012, vol. 43A, pp. 3264–82.
13. B. Zhang, J. Cui, and G. Lu: *Mater. Sci. Eng. A*, 2003, vol. 355, pp. 325–30.
14. C. Stelian, Y. Delannoy, Y. Fautrelle, and T. Duffar: *J. Cryst. Growth*, 2004, vol. 266, pp. 207–15.
15. G.M. Poole, M. Heyen, L. Nastac, and N. El-Kaddah: *Metall. Mater. Trans. B*, 2014, vol. 45A, pp. 1834–41.
16. B.D. Cullity and C.W. Allen: *Acta Metall.*, 1965, vol. 13, pp. 933–35.
17. X. Liu, J. Cui, X. Wu, Y. Guo, and J. Zhang: *Scripta Mater.*, 2005, vol. 52, pp. 79–82.
18. X. Hu, L. Peng, S. Qian, P. Fu, and W. Ding: *Mater. Lett.*, 2014, vol. 123, pp. 238–41.
19. X. Liu, J. Cui, E. Wang, and J. He: *Mater. Sci. Eng. A*, 2005, vol. 402, pp. 1–4.
20. Y.Z. Liu, L.H. Zhan, Q.Q. Ma, Z.Y. Ma, and M.H. Huang: *J. Alloys Compd.*, 2015, vol. 647, pp. 644–47.
21. C. Li, G. Guo, Z. Yuan, W. Xuan, X. Li, Y. Zhong, and Z. Ren: *J. Alloys Compd.*, 2017, vol. 720, pp. 272–76.
22. M. Flemings, D. Poirier, R. Barone, and H. Brody: *J. Iron Steel Inst.*, 1970, vol. 208, pp. 371–81.
23. M.N. Gungor: *Metall. Trans. A*, 1989, vol. 20A, pp. 2529–33.
24. M. Ganesan, D. Dye, and P. Lee: *Metall. Mater. Trans. A*, 2005, vol. 36A, pp. 2191–2204.
25. M. Seyring, X. Song, and M. Rettenmayr: *ACS Nano*, 2011, vol. 5, pp. 2580–86.
26. R. Völkl, U. Glatzel, and M. Feller-Kniepmeier: *Acta Mater.*, 1998, vol. 46, pp. 4395–4404.
27. A.G. Khachaturyan, S.V. Semenovskaya, and J.W. Morris: *Acta Metall.*, 1988, vol. 36, pp. 1563–72.
28. T. Miyazaki and M. Doi: *Mater. Sci. Eng. A*, 1989, vol. 110, pp. 175–85.
29. A.A. Hopgood and J.W. Martin: *Mater. Sci. Technol.*, 1986, vol. 2, pp. 543–46.
30. J. Lapin, M. Gebura, T. Pelachová, and M. Nazmy: *Kovove Mater.*, 2008, vol. 46, pp. 313–22.
31. N. Warnken, D. Ma, A. Drevermann, R.C. Reed, S.G. Fries, and I. Steinbach: *Acta Mater.*, 2009, vol. 57, pp. 5862–75.
32. R. Schmidt and M. Feller-Kniepmeier: *Scripta Metall.*, 1992, vol. 26, pp. 1919–24.
33. F. Pyczak, B. Devrient, and H. Mughrabi: *Superalloys*, 2004, vol. 2004, pp. 827–36.
34. Y. Mishima, S. Ochiai, and T. Suzuki: *Acta Metall.*, 1985, vol. 33, pp. 1161–69.
35. J.K. Tien and R.P. Gamble: *Metall. Trans.*, 1972, vol. 3A, pp. 2157–62.
36. T. Murakumo, T. Kobayashi, Y. Koizumi, and H. Harada: *Acta Mater.*, 2004, vol. 52, pp. 3737–44.
37. R.C. Reed, D.C. Cox, and C. Rae: *Mater. Sci. Technol.*, 2007, vol. 23, pp. 893–902.
38. I.M. Lifshitz and V.V. Slyozov: *J. Phys. Chem. Solids*, 1961, vol. 19, pp. 35–50.
39. C. Wagner: *Z. Elektrochem.*, 1961, vol. 65, pp. 581–91.
40. Y. Zhang, N. Gey, C. He, X. Zhao, L. Zuo, and C. Esling: *Acta Mater.*, 2004, vol. 52, pp. 3467–74.
41. G. Urbain and E. Übelacker: *Adv. Phys.*, 1967, vol. 16, pp. 429–38.
42. F.R. de Boer, C.J. Schinkel, J. Biesterbos, and S. Proost: *J. Appl. Phys.*, 1969, vol. 40, pp. 1049–55.
43. A.J. Ardell and V. Ozolins: *Nat. Mater.*, 2005, vol. 4, pp. 309–16.
44. A.J. Ardell: *Interface Sci.*, 1995, vol. 3, pp. 119–25.
45. C. Li, S. He, Y. Fan, H. Engelhardt, S. Jia, W. Xuan, X. Li, Y. Zhong, and Z. Ren: *Appl. Phys. Lett.*, 2017, vol. 110, p. 074102.
46. C. Li, S. He, H. Engelhardt, T. Zhan, W. Xuan, X. Li, Y. Zhong, Z. Ren, and M. Rettenmayr: *Sci. Rep.*, 2017, vol. 7, p. 18085.
47. M. Karunaratne, D.C. Cox, P. Carter, and R.C. Reed: *Superalloys*, 2000, vol. 2000, pp. 263–72.
48. J. Tiley, G.B. Viswanathan, R. Srinivasan, R. Banerjee, D.M. Dimiduk, and H.L. Fraser: *Acta Mater.*, 2009, vol. 57, pp. 2538–49.
49. J. Lapin, M. Gebura, O. Bajana, T. Pelachová, and M. Nazmy: *Kovove Mater.*, 2009, vol. 47, pp. 129–38.

50. A.J. Ardell: *Metall. Mater. Trans. B*, 1970, vol. 1A, pp. 525–34.
51. T. Miyazaki, H. Imamura, H. Mori, and T. Kozakal: *J. Mater. Sci.*, 1981, vol. 16, pp. 1197–1203.
52. R.A. Ricks, A.J. Porter, and R.C. Ecob: *Acta Metall.*, 1983, vol. 31, pp. 43–53.
53. M.F. Henry, Y.S. Yoo, D.Y. Yoon, and J. Choi: *Metall. Trans. A*, 1993, vol. 24A, pp. 1733–43.
54. Mats. Hillert: *Phase Equilibria, Phase Diagrams and Phase Transformations: Their Thermodynamic Basis*, Cambridge University Press, Cambridge, 2007.
55. J.H. Westbrook: *Z. Kristallogr.*, 1958, vol. 110, p. 21.
56. T. Miyazaki, H. Imamura, and T. Kozakai: *Mater. Sci. Eng.*, 1982, vol. 54, pp. 9–15.
57. A. Hazotte, T. Grosdidier, and S. Denis: *Scripta Mater.*, 1996, vol. 34, pp. 601–08.
58. M. Feller-Kniepmeier, T. Link, I. Poschmann, G. Scheunemann-Frerker, and C. Schulze: *Acta Mater.*, 1996, vol. 44, pp. 2397–2407.
59. C.T. Sims, N.S. Stoloff, and W.C. Hagel: *Superalloys II*, Wiley, New York, 1987.
60. E. Fleischmann, M.K. Miller, E. Affeldt, and U. Glatzel: *Acta Mater.*, 2015, vol. 87, pp. 350–56.
61. A.J. Ardell: *Metall. Trans. A*, 1985, vol. 16A, pp. 2131–65.
62. R.C. Reed: *The Superalloys Fundamentals and Applications*, Cambridge University Press, Cambridge, 2006.
63. B. Reppich: *Acta Metall.*, 1982, vol. 30, pp. 87–94.
64. R.O. Scattergood and D.J. Bacon: *Philos. Mag.*, 1975, vol. 31, pp. 179–98.
65. P. Beauchamp, J. Douin, and P. Veyssiere: *Philos. Mag. A*, 1987, vol. 55, pp. 565–81.
66. S.M. Copley and B.H. Kear: *Trans. TMS AIME*, 1967, vol. 239, pp. 984–92.
67. H. O'Neill: *Hardness Measurement of Metals and Alloys*, Chapman & Hall, London, 1967.
68. W.W. Milligan and S.D. Antolovich: *Metall. Trans. A*, 1987, vol. 18A, pp. 85–95.
69. A. Sengupta, S.K. Putatunda, L. Bartosiewicz, J. Hangas, P.J. Nailos, M. Peputapeck, and F.E. Alberts: *J. Mater. Eng. Perform.*, 1994, vol. 3, pp. 73–81.